UNIVERSITY OF LEEDS

This is a repository copy of *Analysis of time-lapse travel-time and amplitude changes to assess reservoir compartmentalization*.

White Rose Research Online URL for this paper:
http://eprints.whiterose.ac.uk/82323/

Version: Accepted Version

Article:
He, Y, Angus, DAC orcid.org/0000-0003-0734-7835, Clark, RA orcid.org/0000-0002-3508-8183 et al. (1 more author) (2016) Analysis of time-lapse travel-time and amplitude changes to assess reservoir compartmentalization. Geophysical Prospecting, 64 (1). pp. 54-67. ISSN 0016-8025

https://doi.org/10.1111/1365-2478.12250

Reuse
Items deposited in White Rose Research Online are protected by copyright, with all rights reserved unless indicated otherwise. They may be downloaded and/or printed for private study, or other acts as permitted by national copyright laws. The publisher or other rights holders may allow further reproduction and re-use of the full text version. This is indicated by the licence information on the White Rose Research Online record for the item.

Takedown
If you consider content in White Rose Research Online to be in breach of UK law, please notify us by emailing eprints@whiterose.ac.uk including the URL of the record and the reason for the withdrawal request.

White Rose university consortium
Universities of Leeds, Sheffield & York

eprints@whiterose.ac.uk
https://eprints.whiterose.ac.uk/

Analysis of time-lapse travel-time and amplitude changes to assess reservoir compartmentalization

Y-X. He*, D.A. Angus, R.A. Clark and M.W. Hildyard

School of Earth & Environment, University of Leeds, Leeds, LS2 9JT, United Kingdom.

E-mail: eeyhe@leeds.ac.uk.

ABSTRACT

Fluid depletion within a compacting reservoir can lead to significant stress and strain changes and potentially severe geomechanical issues, both inside and outside the reservoir. We extend previous research of time-lapse seismic interpretation by incorporating synthetic near-offset and full-offset common-midpoint reflection data using anisotropic ray tracing to investigate uncertainties in time-lapse seismic observations. The time-lapse seismic simulations use dynamic elasticity models built from hydro-geomechanical simulation output and a stress-dependent rock physics model. The reservoir model is a conceptual two-fault graben reservoir, where we allow the fault fluid-flow transmissibility to vary from high to low to simulate non-compartmentalized and compartmentalized reservoirs respectively. The results indicate time-lapse seismic amplitude changes and traveltime shifts can be used to qualitatively identify reservoir compartmentalization. Due to the high repeatability and good quality of the time-lapse synthetic dataset, the estimated traveltime shifts and amplitude changes for near-offset data match the true model subsurface changes with minimal errors. A 1D velocity-strain relation was used to estimate the vertical velocity change for the reservoir bottom interface by applying zero-offset time-shifts from both the near-offset and full-offset measurements. For near-offset data, the estimated P-wave velocity changes were within 10% of the true value. However, for full-offset data, time-lapse attributes are quantitatively reliable using standard time-lapse seismic methods when an updated velocity model is used rather than the baseline model.

Key words: Time-lapse seismic estimates, Waveform modelling, Reservoir compartmentalization.

1 INTRODUCTION

Reservoir production can cause serious geomechanical issues in a reservoir and the surrounding rocks, especially when strong stress and strain changes occur. Reservoir compaction due to declining pore

pressure inside a producing reservoir has been observed in a number of reservoirs in the Gulf of Mexico and North Sea, particularly in the high-porosity, over-pressured (HPHT) sand and chalk reservoirs with large thickness (e.g., Guilbot and Smith 2002; Hawkins *et al*. 2007; Herwanger and Horne 2009). Reservoir compaction due to production can act as a major driving mechanism for fluid flow by maintaining pressure. Due to reservoir heterogeneity and geometry, hydrocarbon production can lead to reservoir compartmentalization and subsequent heterogeneous pore pressure distribution. Furthermore, large strain and stress changes in the overburden might lead to wellbore failure due to shear or fault reactivation and hence cause serious economic loss. Monitoring and understanding stress and reservoir pressure changes across faults (or any barrier) is therefore of considerable significance to avert drilling and reservoir depletion related problems.

Time-lapse seismic monitoring of production-induced changes in a reservoir and the surrounding rocks over time has the basic aim of mapping reservoir compartments and subsurface rock deformation, identifying by-passed oil, monitoring fluid movement and planning for future production performance (e.g., Calvert 2005; Herwanger and Koutsabeloulis 2011). The general idea behind the time-lapse seismic approach is to enable separation of the effects of fluid saturation and pore pressure changes, and this has been challenging (Landrø 2001; Trani *et al*. 2011; MacBeth *et al*. 2011). Since reservoir compaction and pore pressure changes induced by fluid depletion in a reservoir might lead to changes in seismic velocities and layer thickness, it is thus crucial to discriminate between the two effects using time-lapse seismic analysis.

Using a 1D expression to describe the travel-time difference due to geomechanical effects (equation 1, Landrø and Stammeijer 2004), Hatchel and Bourne (2005) and Røste, Stovas and Landrø (2005) propose a linearized relation to link changes in layer velocity and thickness using a dilation factor. Using the dilation factor and assuming uniaxial deformation, vertical velocity change and average vertical strain can be estimated from observed time-lapse vertical travel-time shifts. Moving beyond uniaxial deformation, Minkoff *et al*. (2004) apply coupled fluid-flow and geomechanical simulations capable of predicting production-induced triaxial (3D) stress evolution and deformation within a compacting reservoir. Herwanger and Horne (2009) extend this workflow to predict induced seismic anisotropy and velocity changes due to 3D stress and strain evolution within and outside a reservoir. Herwanger and Horne (2009) use a third-order elasticity rock physics model (Prioul, Bakulin and

Bakulin 2004) to estimate seismic velocity perturbations caused by production induced effective stress changes. Fuck, Bakulin and Tsvankin (2009) and Fuck, Tsvankin and Bakulin (2011) introduce an analytic geomechanical model with third-order elasticity to predict travel-time shifts due to stress-induced seismic velocity heterogeneity and anisotropy within and surrounding a compacting reservoir. Verdon *et al*. (2008) and Angus *et al*. (2009) and Angus, Fisher and Verdon (2012) extend and calibrate a micro-structural rock-physics approach to model the nonlinear elastic response due to varying effective stress and hence predict induced changes in seismic velocity and anisotropy. Verdon *et al*. (2011) and Angus *et al*. (2011) integrate the micro-crack rock physics model with coupled fluid-flow and geomechanical simulation (Segura *et al*. 2011) for seismic modelling applications to evaluate various time-lapse seismic and microseismic attributes. The primary reason for using the micro-crack model rather than the third-order elasticity model is based on practical considerations; most ultrasonic stress-dependent velocity measurements do not include the strain measurements needed for third-order elasticity theory.

In spite of many successful applications of the time-lapse seismic technique for reservoir monitoring (Barkved 2012) and hydro-geomechanical calibration (Herwanger *et al*. 2010), various uncertainties exist. These uncertainties exist for several reasons, but primarily they relate to the fact that the hydro-geomechanical and rock physics models are simplified representations of the true physics. Furthermore, there is the question of how best to process time-lapse seismic data. Smith and Tsvankin (2012) analyze the stress and strain-induced travel-time shifts using coupled fluid-flow and geomechanical simulation, third-order elasticity rock physics model and multicomponent full-waveform finite-difference seismic modeling. To the authors' knowledge, Smith and Tsvankin (2012) provide the first study using full waveform synthetic data to develop a processing workflow that includes f-k (frequency-wavenumber) filtering of shot records, cross-correlation skip corrections and an adaptive polynomial time-shift curve fitting. The integration of time-lapse seismic analysis and hydro-geomechanical simulation can strengthen our understanding of the evolution of the dynamic reservoir system, and hence lead to a better quantification of trapped oil, optimization of well placement and design, and hydrocarbon extraction procedure.

In this paper we use ray-based waveform forward modelling to investigate the fidelity of time-lapse seismic processing to extract time-lapse seismic attributes, and whether these attributes can credibly

be used to identify reservoir compartmentalization. The ray-based synthetics allow us to avoid complications from multiple energy in the processing as well as provide fast synthetic waveforms for 3D generally anisotropic velocity models. The dynamic elastic models constructed from hydro-geomechanical simulation and non-linear micro-crack rock physics models are considered the ground-truth model. Estimated time-lapse seismic attributes (travel-time shifts and reflection amplitude changes) are compared with the dynamic elastic models to study the effects of errors resulting from time-lapse seismic processing and time-lapse seismic attribute calculations. Understanding these errors is necessary for meaningful calibration of hydro-geomechanical models and improving subsurface reservoir predictions. A major objective of this study is to develop a method of being able to study, both qualitatively and quantitatively, the influences of these errors in time-lapse seismic observations by using an integrated fluid-flow and geomechanical simulation, rock physics model and seismic simulation.

2 METHODOLOGY

In time-lapse seismic studies, there are two approaches to reduce uncertainty in reservoir predictions and enhance the imaging quality of by-passed reserves (Davies and Maver 2004): *simulation to seismic* and *seismic to simulation*. In both approaches, the workflow requires the integration of hydro-geomechanical simulation, rock physics models and time-lapse seismic analysis. To quantitatively monitor and measure small subsurface physical changes, we need to understand the magnitude of errors inherent in time-lapse seismic analysis and hence how much the true time-lapse changes might be over-predicted or under-predicted due to these errors.

[FIGURE 1 HERE]

In this paper, we focus on developing the forward modelling (*simulation to seismic*) approach (see Figure 1). Specifically, the dynamic elastic models at three stages of production (baseline survey, 5-year and 10-year monitor surveys) are used as the input elastic models for 3D seismic waveform simulation. The waveform synthetics are processed using various methodologies and subsequently compared directly with the dynamic elastic models to evaluate the errors in the conventional time-lapse estimates, and hence potential errors and uncertainties in the time-lapse seismic observations (He *et al*. 2013). In principle, deviations between the synthetics and the true time-lapse seismic attributes could be influenced by the waveform simulation algorithm (anisotropic ray theory) and the

rock physics model, but it is expected that the major influence will be due to the band-limited nature of seismic waveforms (i.e., resolution), acquisition geometry and time-lapse seismic processing.

2.1 Two-fault graben reservoir model

The subsurface model we use in this study is a graben-style reservoir consisting of three reservoir compartments separated by two normal faults (Angus *et al*. 2010; Lynch *et al*. 2013). Two production cases are examined, one having high fault fluid-flow transmissibility (HFT) and the other having low fault fluid-flow transmissibility (LFT). Figure 2 shows the geometry of the model, with the production well located in the centre of the left-most reservoir compartment. Hydro-geomechanical simulation is performed using two-way iteratively coupled reservoir flow simulator Tempest with geomechanical solver Elfen (Segura *et al*. 2011), where the geomechanical simulator uses pore pressure evolution calculated in the reservoir simulator to update the geomechanical loading and the reservoir simulator uses the updated pore volume change calculated in the geomechanical simulator to update the flow properties. In the simulation, the production well is produced at a constant rate of 4000 m^3/day at a minimum well pressure of 5 MPa over the duration of the simulation. The stress, pressure and static elastic tensor are output every six months of simulation time and are used as input for the non-linear rock physics model of Verdon *et al*. (2008) to construct the dynamic elastic models for waveform simulation (Angus *et al*. 2011).

[FIGURE 2 HERE]

Since the hydro-geomechanical mesh is unstructured, the dynamic elastic model is discretised on an appropriate regular grid with arbitrary spatial density suitable for ray tracing via a B-spline interpolation algorithm. As well, since ray tracing requires a smooth velocity model, the elastic model is also smoothed using a damped least squares method to remove sharp interfaces as well as sharp transitions in elastic properties. Figure 3 shows an example of the 3D P-wave velocity model after interpolation and smoothing. Also shown in Figure 3 is a 1D P-wave velocity profile through the centre of the left reservoir-compartment that compares the original, interpolated and smoothed velocities.

[FIGURE 3 HERE]

Given the asymmetry and heterogeneity of the graben model, stress perturbations will be triaxial and hence seismic anisotropy will develop (e.g., Herwanger and Koutsabeloulis 2011). To investigate the

influence of induced seismic anisotropy as well as induced velocity heterogeneity on estimated time-lapse seismic attributes (e.g., Hawkins *et al*. 2007; Herwanger and Horne 2009), both anisotropic elastic models and equivalent isotropic elastic models are constructed. The isotropic model assumes vertical effective stress changes only, and hence the elastic tensor C_{33} is used to compute the P-wave velocity.

2.2 Acquisition geometry and waveform synthetics

An anisotropic ray tracer (Guest and Kendall 1993) is used to generate seismic synthetics. The simulation uses both ray shooting (variable incidence and azimuth angles) and normal incidence (e.g., exploding reflector method) modes. Figure 4 shows an example of the ray shooting method for one shot with various incidence angles and tracking two reflectors; in this paper we focus on the top and bottom reservoir layers (two red interfaces) to examine the time-lapse seismic responses due to triaxial effective stress changes and strain within and outside the reservoir. P-wave explosive point sources were simulated using a zero-phase Ricker wavelet with central frequency of 30 Hz and temporal sample of 1 ms, positioned along the surface and down the centre of the long-axis (x-direction) of the model. The source-receiver offsets vary from 0 m to 5500 m, with receiver spatial spacing of 12.5 m.

[FIGURE 4 HERE]

The synthetic shot gather data are resorted into common-mid point (CMP) gathers, normal-moveout (NMO) corrected, stacked and time-migrated using the Stolt migration method. Figure 5 shows a post-stack migrated image of baseline model using the reflections from the two reservoir layers. Identical acquisition geometry, source wavelet and processing procedures were applied to the baseline, 5-year monitor (monitor1) and 10-year monitor (monitor2) surveys such that time-lapse seismic repeatability is not an issue with the subsequent analysis. Although it is expected that the post-stack near-offset data will provide better vertical resolution of time-lapse seismic changes than post-stack full-offset data (due to offset effects), the post-stack full-offset data should contain more information on induced lateral velocity heterogeneity within the subsurface. Since near-offset data contains mainly sub-vertically propagating energy, the information carried by near-offset reflections will be dominated by vertical velocity variation. Full-offset data contain sub-vertical as well as oblique incident reflections and so will contain information dominated by vertical and lateral velocity variation. To ground-truth the

near- and full-offset time-lapse reflection seismic analysis with the true dynamic elastic model for both isotropic and anisotropic medium, we use vertical incidence synthetics (utilizing the normal incidence ray tracing) to provide the benchmark travel-time shifts and reflection amplitude changes.

[FIGURE 5 HERE]

2.3 Calculation of time-lapse seismic attributes

The standard time-lapse seismic attribute, travel-time shift, is calculated by cross-correlation of the baseline and monitor surveys. We use a Hanning window with length of 80 ms and 66 ms for the top and bottom reservoir horizons (such that the window length encompasses the reflection events that have approximate period of 70 ms and 50 ms for the top and bottom horizons respectively). The time-shift is calculated by interpolating the time lag for maximum cross-correlation (i.e., to improve the resolution of estimated travel-time shifts). The reflection amplitude changes are estimated first by correcting for the travel-time shift between traces and then calculating the difference between the maximum reflection amplitudes of both traces (see Figure 6). Previous studies (e.g., Hodgson 2009; Selwood 2010; Whitcombe *et al*. 2010) have shown that the conventional cross-correlation technique is not ideal for time-lapse seismic travel-time shift analysis. This is because travel-time shift recovery using cross-correlation is dependent on window length (Selwood 2010), which could lead to high-frequency noisy or incorrect estimates (Whitcombe *et al*. 2010). However, in this study we are primarily concerned with the general recovery of time-lapse seismic attributes and so do not apply more advanced methods of estimating time shifts.

[FIGURE 6 HERE]

3 Results: time-lapse seismic attributes

The reflection amplitudes estimated from the baseline, monitor1 and monitor2 surveys for both isotropic and anisotropic HFT models are displayed in Figure 7. The amplitudes are normalised to the largest magnitude of the baseline anisotropic model (in this case the largest amplitudes are for the left and right top reservoir interface). The difference in amplitude change estimates between near-offset data and the ground-truth is less than 10%. However, the difference in amplitude change estimates using the full-offset data shows significantly larger deviations ranging between 20% and 50%, especially in the left and right reservoir compartments.

The reflection coefficients along the reservoir interfaces are influenced by fluid depletion induced pore pressure changes (we do not model saturation effects so that we can focus solely on pressure effects). The absolute amplitude decrease indicates a velocity increase in the reservoir and decrease in the surrounding overburden and under-burden (i.e., reservoir velocities approach that of the surrounding rock). There is little difference in the magnitude of amplitude changes in the isotropic and the anisotropic models (see Figure 7), and this suggests that induced velocity heterogeneity is more dominant than induced seismic anisotropy. The amplitude changes in the central compartment are significantly less than the left and right compartments (i.e., nearly 10%) as a result of stress arching due to compaction and reservoir geometry (Angus *et al*. 2010). This indicates the importance of recognising stress arching in the time-lapse signature. Assuming uniaxial deformation one might incorrectly assume the central compartment is not as productive compared to the left and right compartments.

[FIGURE 7 HERE]

In Figure 8, the reflection amplitudes calculated from the anisotropic LFT model for monitor1 and monitor2 are displayed. Similar to the HFT model, the reflection amplitudes decrease for both the top and bottom reservoir interfaces, though only in the left compartment (in the right and central compartments the amplitude changes are negligible). This is because the low fluid-flow transmissibility of both faults inhibits fluid flow from the central and right compartments to the production well in the left compartment and hence pore pressure reduction is restricted to the left compartment. The slight observable changes that occur in the central and right compartments relate to stress arching due to stress redistribution in the overburden above the left compartment and fault movement (Angus *et al*. 2010).

[FIGURE 8 HERE]

In Figure 9, the vertical travel-time shifts calculated from the near-offset and full-offset data for the isotropic and anisotropic HFT models are displayed with the ground-truth model. The full-offset travel-time shifts are larger than the near-offset time shifts for both the top and bottom reservoir interfaces (see Figure 9). In monitor1, the travel-time shift estimates are positive for the top interface and negative for the bottom interface. For longer production and hence greater pore pressure reduction in monitor2, travel-time shifts for the bottom interface in the middle compartment transition from negative

(-2 ms) to positive (5 ms). The increase in travel-time from the top interface results from reduced velocity due to overburden extension. The initial decrease in travel-time from the bottom interface results from increased velocity and layer compaction within the reservoir, and the transition to positive shift is due to the evolving stress arching in the overburden.

[FIGURE 9 HERE]

Figure 10 demonstrates the time-lapse seismic travel-time shifts for the anisotropic LFT model. Larger travel-time shift estimates for the full-offset data can be observed compared to the near-offset data (similar to the results shown in Figure 9). The travel-time shifts are limited mainly to the left compartment, though there are small negative travel-time shifts (-1 to -2 ms) over the central and right compartments due to stress arching and reservoir geometry. In monitor2, the development of stress arching in the overburden and side-burden has a significantly larger influence and leads to positive travel-time shifts for the bottom layer.

[FIGURE 10 HERE]

The results from the time-lapse seismic attributes can be summarised as follows:

- The amplitude changes are sensitive to reservoir compaction relatively immediately, not only locally close to the production well but also further away in the other compartments (for the HFT model),
- The time shifts are less sensitive than the amplitude changes to reservoir compaction since amplitude change is a more local attribute whereas time shift is a path-averaged attribute. Since the time shift is a path-averaged attribute, it is effectively smoothed spatially and hence the effect of time shifts away from the producing well can appear delayed temporally. This is the main reason that the time strain attribute is used if the data are not too noisy, since the time strain provides a localised measure of elastic property changes.
- Both amplitude changes and time shifts are sensitive to reservoir compartmentalization, and
- The influence of stress arching has a significant impact on the character of amplitude changes and time shifts, and this relates to the geometry of the reservoir system.

A key observation is that post-stack near-offset seismic data provide a more accurate estimate of time-lapse seismic attributes compared to post-stack full-offset data for conventional 4D seismic processing (i.e., processing workflow that assumes uniaxial deformation). This has more to do with the 4D seismic processing rather than the information contained in mid- and far-offset data. It is clear that pre-stack time-lapse seismic analysis is more appropriate when the subsurface geometry and induced velocity changes show strong lateral heterogeneity and anisotropy.

4 Estimating velocity change using 1D transform

The challenge in time-lapse seismic analysis is to find a suitable approach to discriminate between velocity changes and induced strain, and hence quantitatively differentiate between the influence of fluid saturation, where there is no strain, and reservoir pressure changes. Since travel-time shifts represent the cumulative travel-time differences along the ray path, the seismic travel-time shift attribute will not be a local measure of physical perturbations in the way that reflection amplitudes are. However, the so-called time strain attribute provides an instantaneous (or interval) travel-time difference measurement (Rickett *et al*. 2006) and can be calculated by taking the temporal derivative of time shifts ($\Delta t_0 / t_0$). Landrø and Stammeijer (2004) introduce the zero-offset relative travel-time shift change for a single layer to describe the combined effects of fractional changes in layer thickness and seismic velocity for normal incidence. Assuming $\Delta V / V << 1$ and $\Delta z / z << 1$, Landrø and Stammeijer (2004) write

$$\frac{\Delta t_0}{t_0} \approx \frac{\Delta z}{z} - \frac{\Delta V}{V} = \varepsilon_{zz} - \frac{\Delta V}{V}, \tag{1}$$

where t_0 denotes the vertical two-way travel-time across a thin layer with thickness *z*, *V* is the vertical velocity and $\Delta z / z = \varepsilon_{zz}$ is the average vertical strain over the layer.

Hatchell and Bourne (2005) and Røste *et al*. (2005) introduce a 1D linear model to link vertical strain and velocity changes:

$$\frac{\Delta V}{V} = -R\varepsilon_{zz} = \alpha\varepsilon_{zz}, \tag{2}$$

where the dimensionless factor $R \geq 0$ is the so-called *R*-factor (Hatchell and Bourne 2005) and $\alpha \leq 0$ (Røste *et al*. 2005). The scalar parameter (R or α) represents the relative contribution to time shifts from vertical velocity change and layer thickness change. Although this parameter cannot provide an exact or unique relation between $\Delta V / V$ and ε_{zz}, it has been applied in a wide variety of time-lapse seismic programs.

Hatchell and Bourne (2005) utilize a standard rock velocity-porosity relation with a theoretical crack model to predict values for the dimensionless *R*-factor. The *R*-factor takes on two different values depending on whether the layer is the reservoir unit or the overburden, and this is due to the asymmetrical influence of rock compaction and elongation. Since the velocity-strain factor is assumed to vary over a narrow range (typically between 2 and 3 for the reservoir, and between 4 and 6 in the overburden layers), it has been applied with varying degrees of success on many fields. Herwanger (2008) presents a method to compute the *R*-factor directly using third-order elasticity theory and neglecting horizontal strain changes, yet notes that horizontal stress and strain have a significant effect on vertical velocity changes. The dilator factor α of Røste *et al*. (2005) is dependent on rock properties and can vary spatially. Røste, Landrø and Hatchell (2007) introduce an approach to calculate α from pre-stack seismic data (zero-offset and offset-dependent time shifts) for all offsets within a given layer, and extend it to handle both lateral and vertical changes in thickness and velocity.

[FIGURE 11 HERE]

The estimated vertical P-wave velocity changes using the 1D velocity-strain model of Hatchell and Bourne (2005) and the time strain attribute for the bottom reservoir interface of the HFT and LFT models are shown in Figure 11. We compare velocity change estimates using the near-offset travel-time shifts for four constant *R*-factors: (1) *R*=0 representative of no reservoir compaction or zero strain (solid blue line), (2) *R*=1 for a value smaller than typically used for reservoirs and where velocity and strain changes have equal influence on travel-time shifts (dashed blue line), (3) *R*=3 representative of a value typically applied for reservoirs (solid red line), and (4) *R*=13 for a value larger than typically used for reservoirs and where the time shift contribution is much larger for velocity change with respect to strain change (dashed red line).

Comparing the estimated P-wave velocity changes with the true subsurface model it can be seen that the constant non-zero *R*-factor cases provide a much more reliable estimate of velocity change (e.g., ±20% error for *R*=3 compared to ±80% error for *R*=0) for both the HFT and LFT models. For the HFT model, the estimated P-wave velocity changes for the constant non-zero *R*-value approaches that of the true model in the central compartment with some deviations in the left and right compartments, while the velocities estimated using zero strain *R*-value display large deviations (between ±30% to ±80% error) throughout the reservoir. This is consistent with the fact that compaction in the reservoir is not homogeneous due to reservoir geometry and stress arching, and provides strong support for allowing lateral variation in the dilation parameter (Røste *et al*. 2007). The estimated P-wave velocity changes in monitor1 for the LFT model match well with the true model for the constant non-zero *R*-values (within ±10% error). However, the velocity predictions worsen (±50% error) due to production-related stress and strain heterogeneity after a longer period of production. The chosen constant *R*-values used in the HFT models are larger than in the LFT models in order to yield similar velocity predictions to the true model (the low fault transmissibility cases are approximately 50% the high transmissibility cases). The different *R*-values relate to the varying amount of stress arching in the overburden as well as magnitude of stress changes and strains in the reservoir.

Although the constant *R*-value approach yields vertical P-wave velocity change estimates with broad similarity to the true subsurface model, the differences between the estimated and the true subsurface models can still lead to serious errors when predicting fluid properties and stress changes to calibrate hydro-geomechanical models. Error in velocity change estimates will propagate into errors in estimating fluid saturation and pressure changes (Landrø 2001; Ribeiro and MacBeth 2004; Kvam and Landrø 2005; Sayers 2006). When reservoir complexity and/or stress arching is expected to be significant, a more accurate calculation of the velocity-strain relation (R or α factor) is required to improve the time-lapse seismic velocity estimates. In the above example, we consider only vertical strain and assume velocity changes have been modelled adequately using the 1D rock physics model. However, induced seismic anisotropy and velocity heterogeneity due to triaxial strain and stress changes within and outside the reservoir indicates that the approach of Røste, Stovas and Landrø (2006) is likely a more appropriate method to estimate a 'laterally' variable velocity-strain coefficient from pre-stack seismic data.

5 Influence of velocity model on time-lapse seismic uncertainty

In conventional time-lapse seismic processing, both the baseline and monitor observations are processed using identical workflows and, in many instances, the same velocity model (i.e., baseline model), as discussed in Landrø and Stammeijer (2004). When the subsurface velocity changes are small or only the near-offset data are used, the estimated time-lapse seismic travel-time shifts will be quantitatively close to the true model values (e.g., fractional ms error as shown in Figures 9 and 10). However, if the time-lapse velocity changes are significant, accurate velocity analysis for the monitor surveys should be implemented to improve travel-time shift predictions and reduce artificial time-lapse error and uncertainty in the time-lapse seismic attributes. In Figure 12, travel-time shift calculations using the baseline and monitor P-wave velocity models in the stacking and Stolt time-migration procedure are compared. Apparent improvements in the travel-time shifts for the full-offset data using the monitor velocity model are observed and, as expected, very little improvement in the near-offset data. This is because the travel times of full-offset stacks strongly depend on the lateral heterogeneity and non-hyperbolic move-out. Thus, using post-stack full-offset data for time-lapse seismic attribute analysis requires an accurate monitor velocity model when large velocity changes are expected. This is because large velocity changes can cause noticeable time-lapse lateral and vertical shifts through the migrated image (Cox and Hatchell 2008). However, accurate velocity analysis may be either expensive or impractical for time-lapse surveys, and hence the uncertainty in velocity analysis should be incorporated in time-lapse seismic analysis (see Kvam and Landrø 2005).

[FIGURE 12 HERE]

6 CONCLUSIONS

In this study, integrated hydro-geomechanical simulation, rock physics model and waveform seismic simulation is applied to investigate the effects of time-lapse subsurface changes on P-wave attributes. The workflow is applied on a two-fault graben reservoir model with time-variant rock properties due to reservoir production induced effective stress changes inside and outside a reservoir. Travel-time shifts and reflection amplitude changes are used to evaluate physical changes within the reservoir system. The application of time-lapse seismic analysis was helpful to assess reservoir compartmentalization from a qualitative and semi-quantitative estimate. The results indicate that compartmentalization can be identified but that it is important to understand the stress path of the

reservoir if quantitatively accurate estimates are required. Near-offset and full-offset synthetic datasets of high repeatability and quality for baseline and repeated surveys were used to interpret the time-lapse anomalies. The calculated time-lapse P-wave velocities were in general agreement with the true subsurface models when using a constant *R*-value (for both the high and low fault fluid-flow transmissibility models) in the reservoir. Differences in velocity predictions indicate that the producing reservoir is not experiencing uniaxial deformation and that compaction and velocity changes are variable laterally and hence require variable velocity-strain coefficients.

ACKNOWLEDGEMENTS

We would like to thank the associate editor and the two anonymous reviewers for helpful comments to improve the paper. We are grateful to Centre of Integrated Petroleum Engineering and Geoscience, University of Leeds for supporting this work. Y-X. He is supported by a China Scholarship Council/University of Leeds scholarship and D.A. Angus is partially supported by a Research Councils UK Fellowship. We thank Rockfield Software for access to the geomechanical simulator ELFEN, and Roxar for access to the geological model builder RMS (TEMPEST).

REFERENCES

Angus D.A., Fisher Q.J. and Verdon J.P. 2012. Exploring trends in microcrack properties of sedimentary rocks: An audit of dry and water saturated sandstone core velocity-stress measurements. *International Journal of Geosciences* **3**, 822-833.

Angus D.A., Kendall J.M., Fisher Q.J., Segura J.M., Skachkov S., Crook A.J.L. and Dutko M. 2010. Modelling microseismicity of a producing reservoir from coupled fluid-flow and geomechanical simulation. *Geophysical Prospecting* **58**, 901-914.

Angus D.A., Verdon J.P., Fisher Q.J. and Kendall J.M. 2009. Exploring trends in microcrack properties of sedimentary rocks: an audit of dry-core velocity-stress measurements. *Geophysics* **74**, E193-E203.

Angus D.A., Verdon J.P., Fisher Q.J., Kendall J-M., Segura J.M., Kristiansen T.G., Crook A.J.L., Skachkov S., Yu J. and Dutko M. 2011. Integrated fluid-flow, geomechanic and seismic modeling for reservoir characterisation. *Canadian Society of Exploration Geophysicists Recorder* **36**, 26-35.

Barkved O.I. 2012. *Seismic Surveillance for Reservoir Delivery*. EAGE Publications.

Calvert R. 2005. *Insights and Methods for 4D Reservoir Monitoring and Characterization*. EAGE Publications.

Cox B. and Hatchell P. 2008. Straightening out lateral shifts in time-lapse seismic. *First Break* **26**, 93-98.

Davies D. and Maver K.G. 2004. 4D Time-Lapse Studies and Reservoir Simulation to Seismic Modelling. Offshore Technology Conference, Houston, USA, Expanded Abstracts, 16934.

Fuck R.F., Bakulin A. and Tsvankin I. 2009. Theory of traveltime shifts around compacting reservoirs: 3D solutions for heterogeneous anisotropic media. *Geophysics* **74**, D25-D36.

Fuck R.F., Tsvankin I. and Bakulin A. 2011. Influence of background heterogeneity on traveltime shifts for

compacting reservoirs. *Geophysical Prospecting* **59**, 78-89.

Guest W.S. and Kendall J.M. 1993. Modeling seismic waveforms in anisotropic inhomogeneous media using ray and Maslov asymptotic theory: application to exploration seismology. *Canadian Journal of Exploration Geophysics* **29**, 78-92.

Guilbot J. and Smith B. 2002. 4D constrained depth conversion for reservoir compaction estimation: Application to Ekofisk Field. *The Leading Edge* **21**, 302-308.

Hatchell P.J. and Bourne S.J. 2005. Measuring reservoir compaction using time-lapse time shifts. 75th SEG meeting, Houston, USA, Expanded Abstracts, 2500-2503.

Hawkins K., Howe S., Hollingworth S., Conroy G., Ben-Brahim L., Tindle C., Taylor N., Joffroy G. and Onaisi A. 2007. Production-induced stresses from time-lapse time shifts: A geomechanics case study from Franklin and Elgin fields, *The Leading Edge* **26**, 655-662.

He Y-X., Angus D.A., Hildyard M.W. and Clark R.A. 2013. Time-lapse seismic waveform modeling: Anisotropic ray tracing using hydro-mechanical simulation models. 75th EAGE meeting, London, U.K., Expanded Abstracts, We-12-16.

Herwanger J.V. 2008. R we there yet? 70th EAGE meeting, Rome, Italy, Expanded Abstracts, I029.

Herwanger J.V. and Horne S.A. 2009. Linking reservoir geomechanics and time-lapse seismic: Predicting anisotropic velocity changes and seismic attributes. *Geophysics* **74**, W13-W33.

Herwanger J.V. and Koutsabeloulis N. 2011. *Seismic Geomechanics: How to Build and Calibrate Geomechanical Models using 3D and 4D Seismic Data*. EAGE Publications.

Herwanger J.V., Schiøtt C.R., Frederiksen R., If F., Vejbæk O.V., Wold R., Hansen H.J., Palmer E. and Koutsabeloulis N. 2010. Applying time-lapse seismic methods to reservoir management and field development planning at South Arne, Danish North Sea. *Petroleum Geology Conference series*, **7**, 523-535.

Hodgson N. 2009. *Inversion for reservoir pressure change using overburden strain measurements determined from 4D seismic.* PhD Dissertation, Heriot-Watt University.

Kvam Ø. and Landrø M. 2005. Pore-pressure detection sensitivities tested with time-lapse seismic data. *Geophysics* **70**, O39-O50.

Landrø M. 2001. Discrimination between pressure and fluid saturation change from time-lapse seismic data. *Geophysics* **66**, 836-844.

Landrø M. and Stammeijer J. 2004. Quantitative estimation of compaction and velocity changes using 4D impedance and traveltime changes. *Geophysics* **69**, 949-957.

Lynch T., Angus D., Fisher Q. and Lorinczi P. 2013. The impact of geomechanics on monitoring techniques for CO_2 injection and storage. *Energy Procedia* **37**, 4136-4144.

MacBeth C., HajNasser Y., Stephen K. and Gardner A. 2011. Exploring the effect of meso-scale shale beds on a reservoir's overall stress sensitivity to seismic waves. *Geophysical Prospecting* **59**, 90-110.

Minkoff S.E., Stone C.M., Bryant S. and Peszynska M. 2004. Coupled geomechanics and flow simulation for time-lapse seismic modelling. *Geophysics* **69**, 200-211.

Prioul R., Bakulin A. and Bakulin V. 2004. Nonlinear rock physics model for estimation of 3D subsurface stress in anisotropic formations: Theory and laboratory verification. *Geophysics* **69**, 415-425.

Ribeiro C. and MacBeth C. 2004. A petroelastic-based approach to pressure and saturation estimation

using 4D seismic. 66th EAGE meeting, Paris, France, Expanded Abstracted, A042.

Rickett J., Duranti L, Hudson T. and Hodgson N. 2006. Compaction and 4-D time strain at the Genesis Field. 76th SEG meeting, New Orleans, US, Expanded Abstract, 3215-3219.

Røste T., Landrø M. and Hatchell P. 2007. Monitoring overburden layer changes and fault movements from time-lapse seismic data on the Valhall field. *Geophysical Journal International* **170**, 1100-1118.

Røste T., Stovas A. and Landrø M. 2005. Estimation of layer thickness and velocity changes using 4D prestack seismic data. 67th EAGE meeting, Madrid, Spain, Expanded Abstracts, C010.

Røste T., Stovas A. and Landrø M. 2006. Estimation of layer thickness and velocity changes using 4D prestack seismic data. *Geophysics* **71**, S219-S234.

Sayers C. 2006. An introduction to velocity-based pore-pressure estimation. *The Leading Edge* **25**, 1496-1500.

Segura J.M., Fisher Q.J., Crook A.J.L., Dutko M., Yu J.G., Skachkov S., Angus D.A., Verdon J.P. and Kendall J-M. 2011. Reservoir stress path characterization and its implications for fluid-flow production simulations. *Petroleum Geoscience* **17**, 335-344.

Selwood C. 2010. *Researching the optimum bandwidth to extract 4D time shifts*. M.Sc. Dissertation, University of Leeds.

Smith S.S. and Tsvankin I. 2012. Modeling and analysis of compaction-induced traveltime shifts for multicomponent seismic data. *Geophysics* **77**, T221-T237.

Trani M., Arts R., Leeuwenburgh O., and Brouwer J. 2011. Estimation of changes in saturation and pressure from 4D seismic AVO and time-shift analysis. *Geophysics* **76**, C1-C17.

Verdon J.P., Angus D.A., Kendall J-M. and Hall S.A. 2008. The effect of microstructure and nonlinear stress on anisotropic seismic velocities. *Geophysics* **73**, D41-D51.

Verdon J.P., Kendall J-M., White D.J. and Angus D.A. 2011. Linking microseismic event observations with geomechanical models to minimise the risks of storing CO_2 in geological formations. *Earth and Planetary Science Letters* **305**, 143-152.

Whitcombe D.N., Paramo P., Philip N., Toomey A., Redshaw T. and Linn S. 2010. The correlated leakage method – it's application to better quality timing shifts on 4D data. 72nd EAGE meeting, Barcelona, Spain, Expanded Abstracts, B037.

FIGURES:

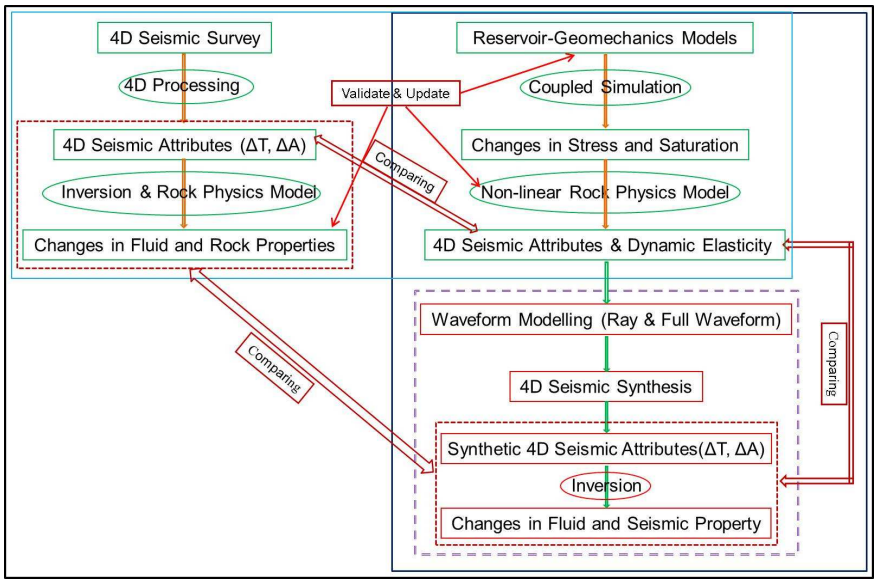

Figure 1 The integrated workflow used in this work. 4D observations can be calibrated at various stages. Previous studies have compared 4D seismic observation directly with hydro-geomechanical models. In this paper, we have developed a workflow that will allow comparing observation with synthetically derived attributes from waveform modelling using the hydro-geomechanical models. This in principal allows an assessment of the 4D seismic resolution and sensitivity of seismic waves to physical changes within the subsurface.

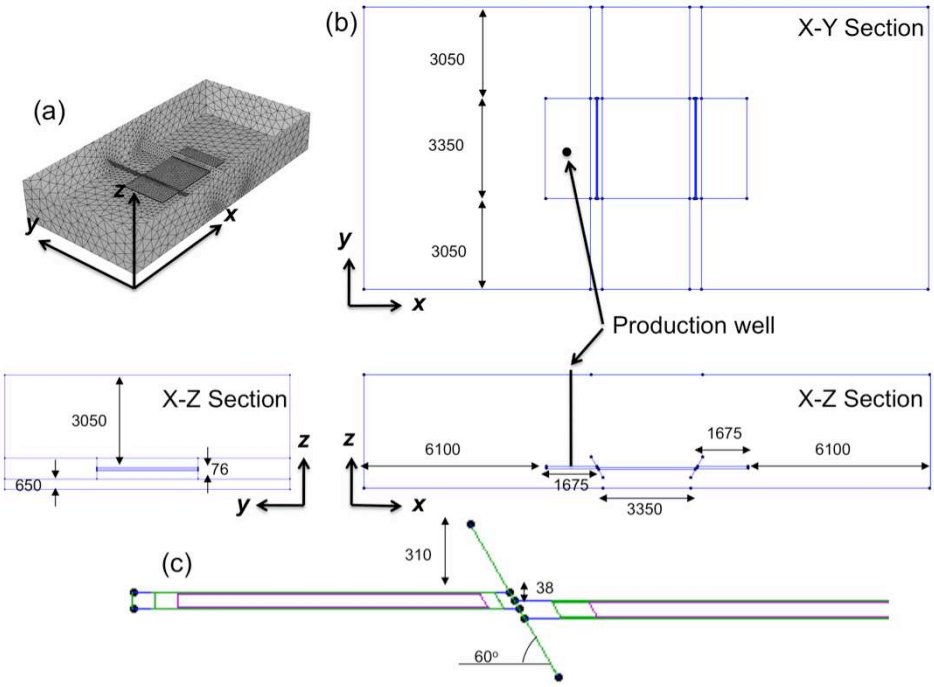

Figure 2 Two-fault graben reservoir model: (a) unstructured geomechanical mesh, (b) vertical and plane-view sections of the reservoir geometry, and (c) geometry of the normal fault intersecting the reservoir layer. X, Y and Z are given in meters.

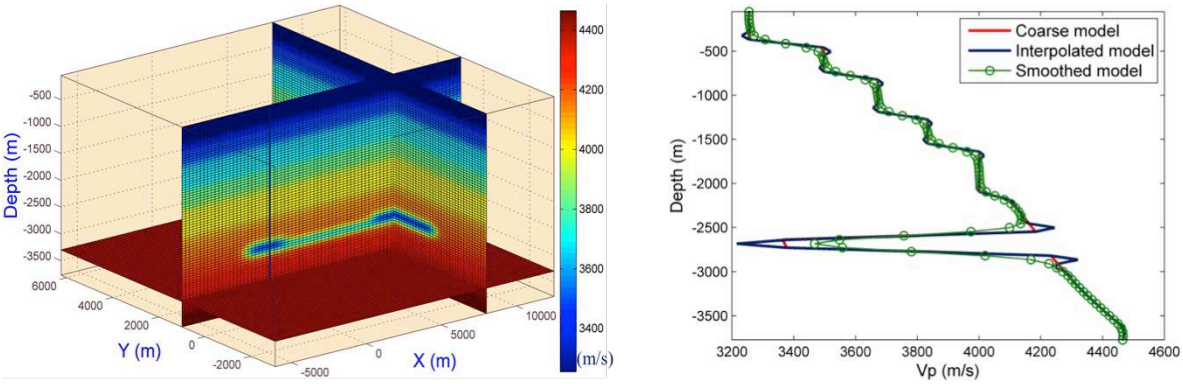

Figure 3 The P-wave velocity model for the two-fault graben reservoir after interpolation and smoothing (left), and 1D P-wave velocity profile (right) through the left compartment (depth profile is along the production well shown by the black line in Figure 2).

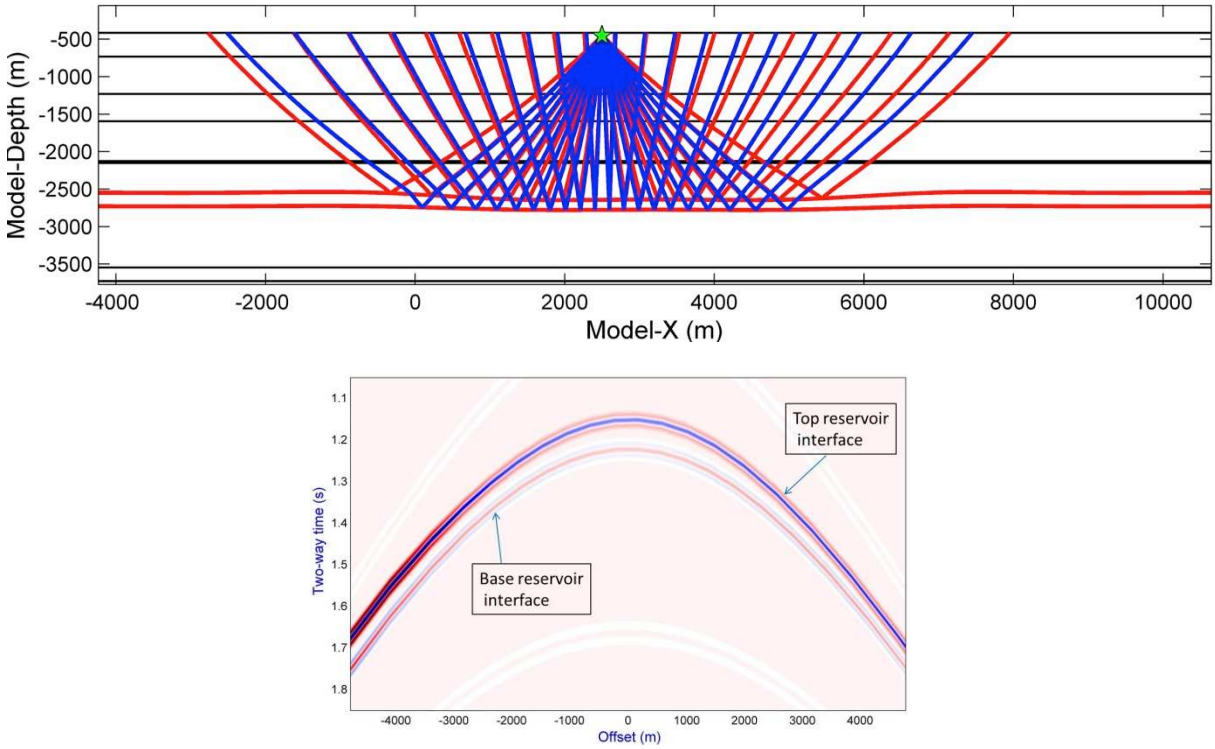

Figure 4 Example of the ray tracing geometry in model (top). Two reflected phases are traced through the model (red rays from the top reservoir interface and blue rays from the bottom reservoir interface) from the top and bottom of the reservoir (shown by the two red line interfaces). Example of a shot gather (bottom) for the source located at 2500 m (see top).

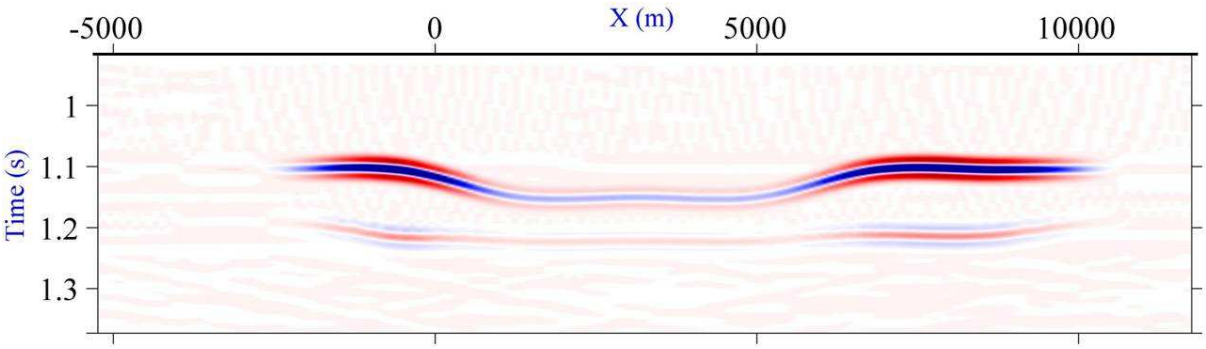

Figure 5 Stolt post-stack migration image of the two-fault graben model using reflections from the top and bottom of the reservoir layers for the baseline survey.

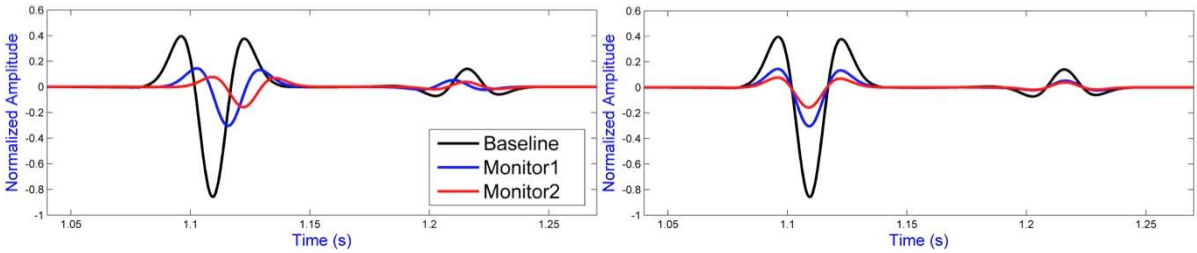

Figure 6 Comparison of seismic traces from the baseline, and the two monitor surveys: before (left) and after (right) time-alignment to the baseline trace.

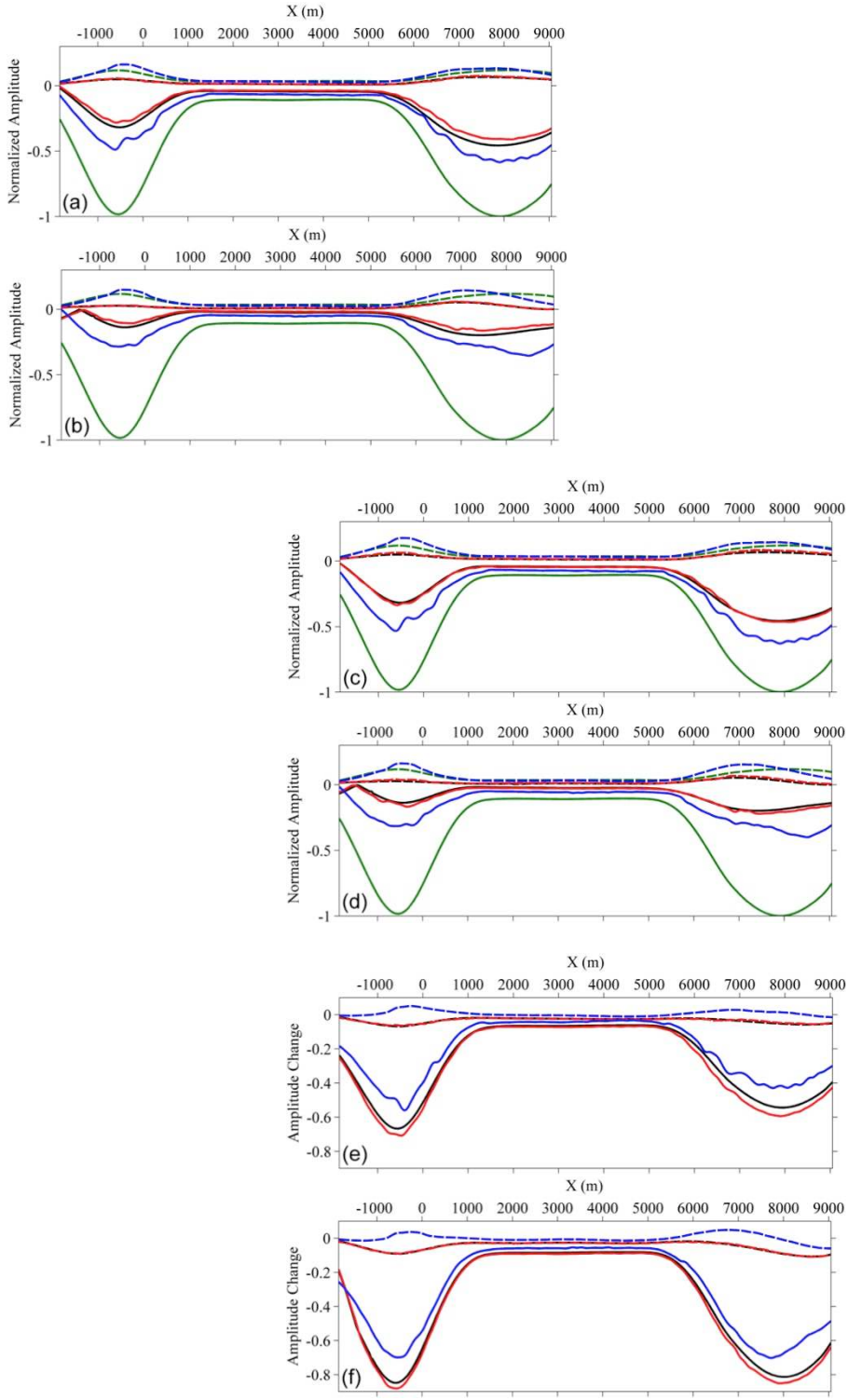
X (m)
-1000 0 1000 2000 3000 4000 5000 6000 7000 8000 9000
Normalized Amplitude
0
-0.5
-1
(a)
(b)
(c)
(d)
Amplitude Change
-0.2
-0.4
-0.6
-0.8
(e)
(f)

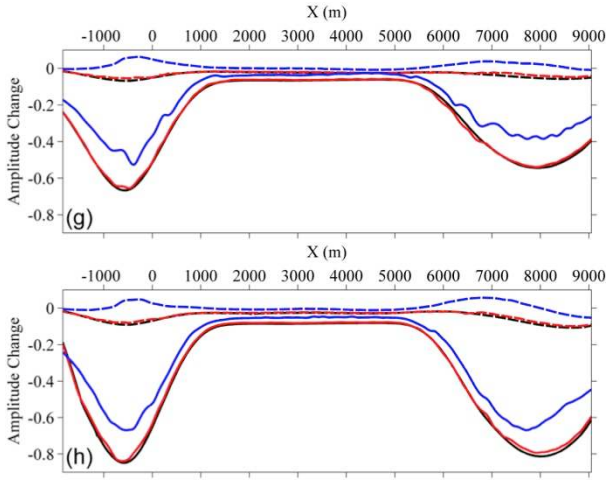

Figure 7 Normalized normal incidence reflection amplitudes of monitor1 (left) and monitor2 (right) survey for HFT model: isotropic model (a) and (b), and anisotropic model (c) and (d). Reflection amplitude changes calculated with respect to the baseline survey: isotropic model (e) and (f), and anisotropic model (g) and (h). The solid lines indicate attributes from the top interface of the reservoir and the dashed lines from the bottom reservoir interface. Colours: green represents normal-incidence baseline, black represents normal-incidence monitor (ground truth), red represents near-offset monitor, and blue represents full-offset monitor.

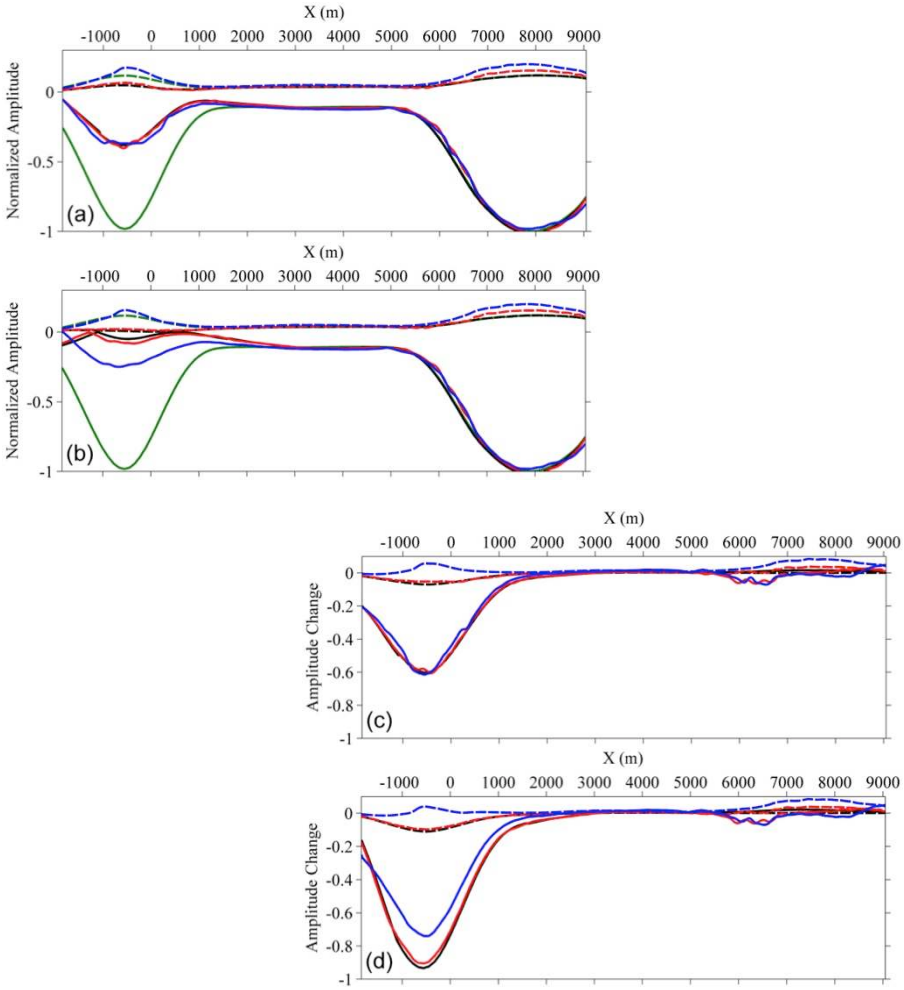

Figure 8 Normalized normal incidence reflection amplitudes ((a) and (b)) of monitor1 (left) and monitor2 (right) for anisotropic LFT model. Changes in reflection amplitude ((c) and (d)) calculated with respect to the baseline model. The solid lines indicate attributes from the top interface of the reservoir and the dashed lines from the bottom reservoir interface. Colours: green represents normal-incidence baseline, black represents normal-incidence monitor (ground truth), red represents near-offset monitor, and blue represents full-offset monitor.

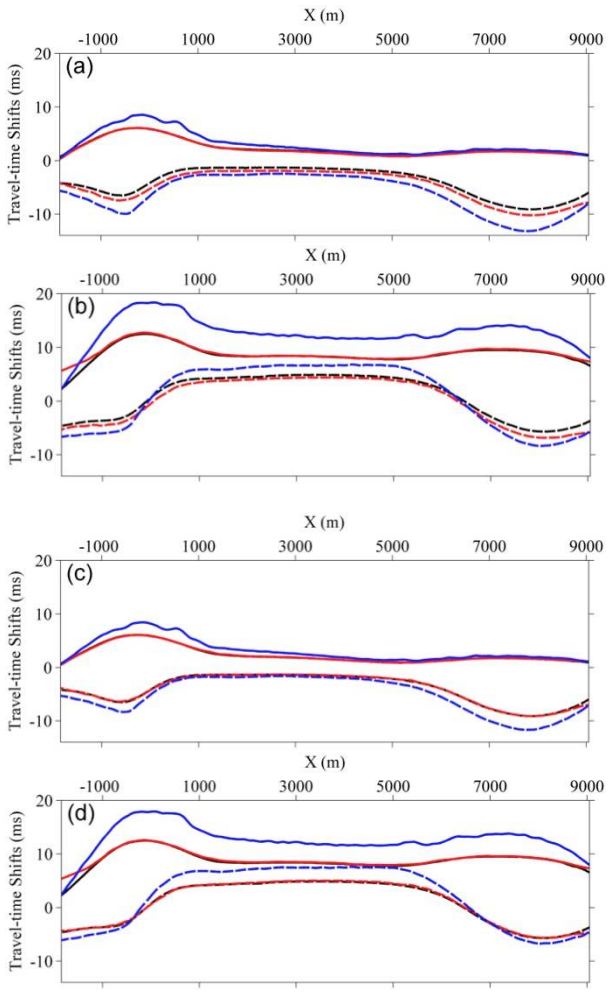

Figure 9 Vertical P-wave travel-time shifts for monitor1 (left) and monitor2 (right) HFT model: isotropic model (a) and (b), and anisotropic model (c) and (d). The solid lines indicate attributes from the top interface of the reservoir and the dashed lines from the bottom reservoir interface. Colours: black represents normal-incidence monitor (ground truth), red represents near-offset monitor, and blue represents full-offset monitor.

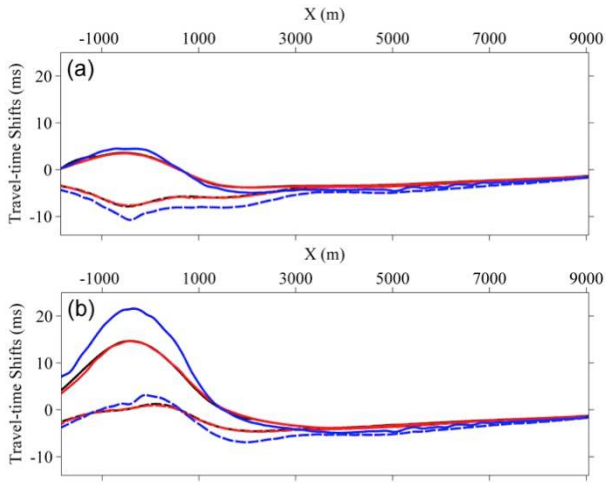

Figure 10 Vertical P-wave travel-time shifts for monitor1 (a) and monitor2 (b) anisotropic LFT model. The solid lines indicate attributes from the top interface of the reservoir and the dashed lines from the bottom reservoir interface. Colours: black represents normal-incidence monitor (ground truth), red represents near-offset monitor, and blue represents full-offset monitor.

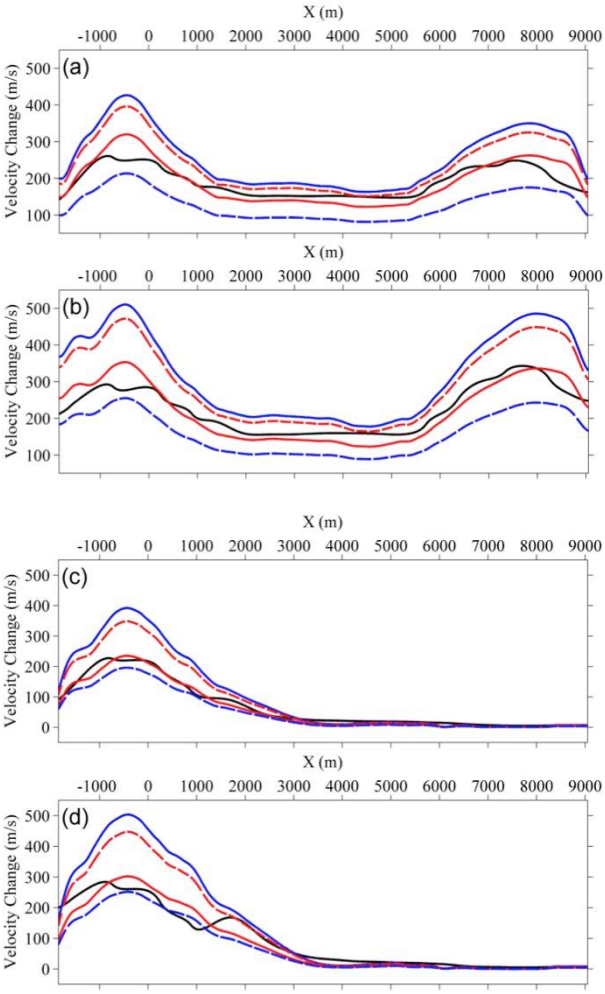

Figure 11 Estimated vertical P-wave velocity changes for the bottom reservoir interface for monitor1 (left) and monitor2 (right) HFT (a) and (b), and LFT (c) and (d) models. The solid black line is the true subsurface model, solid blue line is the constant *R*=0 case, dashed blue line is the *R*=1 case, solid red line is the *R*=3 case, and dashed red line is the *R*=13 case.

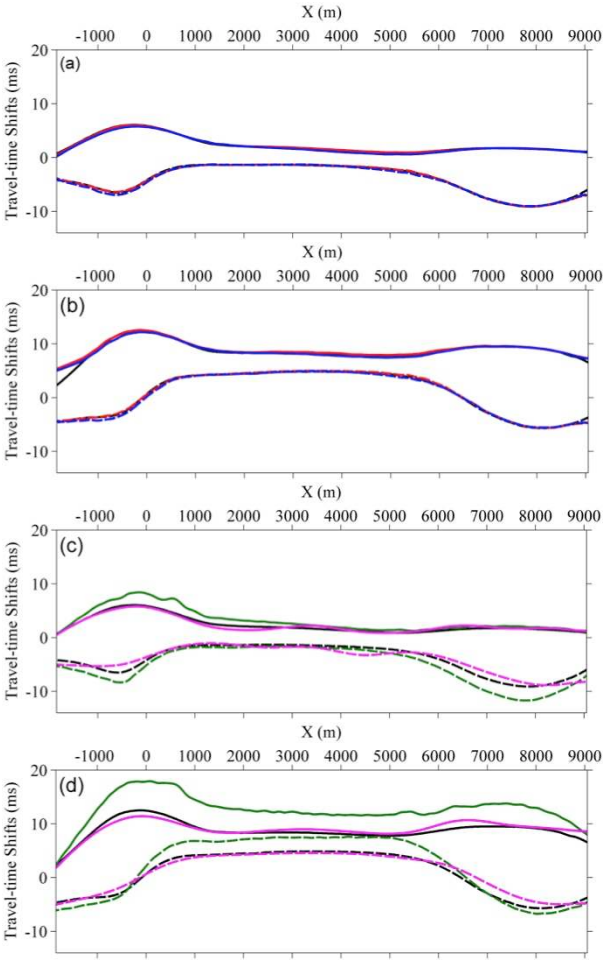

Figure 12 Estimated P-wave vertical time shifts of monitor1 (left) and monitor2 (right) survey; near-offset (top) and full-offset (bottom) dataset. The solid lines indicate travel-time shifts from the top interface of the reservoir and the dashed lines from the bottom reservoir interface. Colours: black represents normal-incidence monitor (ground truth), red represents near-offset monitor survey using Vp of baseline model, blue represents near-offset monitor survey using Vp of monitor model, green represents full-offset monitor survey using Vp of baseline model, pink represents full-offset monitor survey using Vp of monitor model.